

■ Gas-Phase Chemistry | *Hot Paper* |

# Investigation of Cycloparaphenylenes (CPPs) and their Noncovalent Ring-in-Ring and Fullerene-in-Ring Complexes by (Matrix-Assisted) Laser Desorption/Ionization and Density Functional Theory

Martin B. Minameyer,<sup>[a]</sup> Youzhi Xu,<sup>[b]</sup> Stefan Frühwald,<sup>[c]</sup> Andreas Görling,<sup>[c]</sup> Max von Delius,<sup>[b]</sup> and Thomas Drewello<sup>\*[a]</sup>

**Abstract:**  $[n]$ Cycloparaphenylenes ( $[n]$ CPPs) with  $n = 5, 8, 10$  and  $12$  and their noncovalent ring-in-ring and  $[m]$ fullerene-in-ring complexes with  $m = 60, 70$  and  $84$  have been studied by direct and matrix-assisted laser desorption ionization ((MA)LDI) and density-functional theory (DFT). LDI is introduced as a straightforward approach for the sensitive analysis of CPPs, free from unwanted decomposition and without the need of a matrix. The ring-in-ring system of  $[[10]\text{CPP} \supset [5]\text{CPP}]^{++}$  was studied in positive-ion MALDI. Fragmentation and DFT indicate that the positive charge is exclusively located on the inner ring, while in  $[[10]\text{CPP} \supset \text{C}_{60}]^{++}$  it is

located solely on the outer nanohoop. Positive-ion MALDI is introduced as a new sensitive method for analysis of  $\text{CPP} \supset \text{fullerene}$  complexes, enabling the detection of novel complexes  $[[12]\text{CPP} \supset \text{C}_{60, 70 \text{ and } 84}]^{++}$  and  $[[10]\text{CPP} \supset \text{C}_{84}]^{+}$ . Selective binding can be observed when mixing one fullerene with two CPPs or vice versa, reflecting ideal size requirements for efficient complex formation. Geometries, binding and fragmentation energies of  $\text{CPP} \supset \text{fullerene}$  complexes from DFT calculations explain the observed fragmentation behavior.

## Introduction

The first rational synthesis of the cycloparaphenylenes (CPPs)  $[9]$ -,  $[12]$ -, and  $[18]$ CPP was developed in 2008 by Jasti et al.<sup>[1]</sup> Prior to this work, CPPs were only accessible via computational chemistry.<sup>[2]</sup> Meanwhile selective syntheses of numerous other ring sizes and derivatives have evolved and remarkable chemical and physical properties have been revealed.<sup>[3–11]</sup> Due to their structure resembling the shortest unit of an armchair single-walled carbon nanotube (SWCNT), CPPs were used as templates for a bottom-up synthesis of SWCNTs.<sup>[12]</sup> Since CNTs also exist as multi-walled carbon nanotubes (MWCNTs) and form peapod complexes with fullerenes,<sup>[13,14]</sup> similar systems were investigated with the CPPs. Reminiscent of MWCNTs, two CPPs of different sizes can form a ring-in-ring complex. This was first predicted by two independent theoretical studies, which suggested different binding motifs in such a host-guest system, but agreed that binding energies are largest, if the two rings differ by exactly five phenylene units.<sup>[15,16]</sup> Recently, Yamago and co-workers were able to proof these complexes in solution with NMR spectroscopy.<sup>[17]</sup> The host-guest chemistry of strained carbon nanohoops has been reviewed recently.<sup>[18]</sup>


Considerable theoretical and experimental work went into the investigation of the complexation of CPPs with various fullerenes and fullerene derivatives.<sup>[19–29]</sup> Again, Yamago and co-workers were the first to report on the selective formation of a

host-guest complex between  $[10]$ CPP and  $\text{C}_{60}$ , denoted as  $[10]\text{CPP} \supset \text{C}_{60}$ .<sup>[23]</sup> They used NMR to observe the encapsulation. UV/Vis spectroscopy and negative-ion mode atmospheric-pressure chemical-ionization mass spectrometry was employed to verify the 1:1 stoichiometry of the complex. Later, Jasti and co-workers were able to obtain the solid-state structure of the  $[10]\text{CPP} \supset \text{C}_{60}$  complex, providing insight into the different dihedral angles of pristine and complexed  $[10]\text{CPP}$ .<sup>[24]</sup> Yamago and co-workers also achieved the selective complexation of  $\text{C}_{70}$  with  $[10]$ -, and  $[11]$ CPP showing different orientations of the fullerene in either of the CPPs and further achieved the complexation of a diethyl malonate functionalized  $\text{C}_{70}$  with the same rings.<sup>[25]</sup> In a further study, they accomplished the selective formation of a host-guest system consisting of  $[11]$ CPP and  $\text{La}@\text{C}_{82}$ . A ground state charge transfer between the endohedral fullerene and the nanohoop was observed, and the orientation of the encapsulated metal in the host-guest system could be established by the X-ray structure.<sup>[26]</sup> Itami and co-workers investigated the encapsulation of a cationic endohedral fullerene, that is,  $\text{Li}^+@\text{C}_{60}$ , using  $[10]$ CPP as the host. Strong charge transfer was observed between the host and the guest with the charge delocalized over the whole complex.<sup>[27]</sup> Shinohara and co-workers studied endohedral fullerenes of the type  $\text{M}_n@\text{C}_{82}$  and their selective binding to  $[11]$ CPP with spectroscopic methods. Additionally, the selective binding between  $[11]$ CPP and  $\text{M}_n@\text{C}_{82}$  was revealed by laser desorption/ionization (LDI) mass spectrometry. Although the noncovalent complex could not be detected as an intact entity, it was nonetheless possible to identify  $[11]$ CPP and  $\text{M}_n@\text{C}_{82}$  as the two main fragments when laser ablating the precipitate that was formed when  $[11]$ CPP was added to a mixture of “empty” fullerenes and  $\text{M}_n@\text{C}_{82}$ .<sup>[28]</sup> Matrix-assisted laser desorption/ionization (MALDI) time-of-flight MS has been used to characterize a complex consisting of  $\text{C}_{70}$  and a cyclic tetramer of hexa-peri-hexabenzocoronene ( $[4]\text{CHBC}$ ), resembling a  $\pi$ -extended  $[12]$ CPP. This experiment yielded the quasi molecular ion peak of the protonated complex.<sup>[29]</sup> The existence of CPP-based catenanes was recently revealed by combining MALDI with ion mobility mass spectrometry<sup>[30]</sup> and followed by rational synthesis.<sup>[31,32]</sup> The first 2:1 complex placing two  $[10]$ CPPs on the  $(\text{C}_{59}\text{N})_2$  azafullerene dumbbell dimer was recently generated<sup>[33]</sup> and the  $\text{C}_{59}\text{N}^{\bullet}$  radical was successfully stabi-

[a] M. B. Minameyer, Prof. Dr. T. Drewello  
Department of Chemistry and Pharmacy  
Physical Chemistry I  
Friedrich-Alexander University Erlangen-Nürnberg  
Egerlandstrasse 3, 91058 Erlangen (Germany)  
E-mail: thomas.drewello@fau.de

[b] Dr. Y. Xu, Prof. Dr. M. von Delius  
Institute of Organic Chemistry I, University of Ulm  
Albert-Einstein-Allee 11, 89081 Ulm (Germany)

[c] S. Frühwald, Prof. Dr. A. Görling  
Department of Chemistry and Pharmacy, Theoretical Chemistry  
Friedrich-Alexander University Erlangen-Nürnberg  
Egerlandstrasse 3, 91058 Erlangen (Germany)

 Supporting information and the ORCID identification number(s) for the author(s) of this article can be found under:  
<https://doi.org/10.1002/chem.202001503>

lized by supramolecular shielding in the [10]CPP $\supset$ C<sub>59</sub>N<sup>+</sup> complex.<sup>[34]</sup>

Besides the ability to efficiently form noncovalent host-guest complexes with themselves and with fullerenes, other remarkable CPP properties include the fact that the absorption maximum is independent of the ring size and located at approximately 340 nm. This coincides with the excitation wavelength of 337 nm emitted by the nitrogen laser employed in the present study. The Stokes shift, on the other hand, increases with decreasing ring size, while the HOMO–LUMO gap increases with increasing ring size.<sup>[1,4]</sup> This behavior is in contrast to linear paraphenylenes (LPPs).

The present study succeeds recent investigations into the noncovalent charge transfer in porphyrin–[[10]CPP $\supset$ fullerene]-complexes,<sup>[36]</sup> the synthesis of rotaxanes with ring $\supset$ fullerene binding motifs<sup>[37]</sup> and the introduction of a novel CPP/porphyrin-based nano hoop.<sup>[38]</sup> This investigation represents the first comprehensive study employing (MALDI) to the study of CPPs of different ring sizes, their [ring $\supset$ ring]- and [ring $\supset$ fullerene]-complexes. Pristine CPPs are activated at different laser fluences by direct LDI providing insight into the formation of intact molecular ions, their decomposition and fusion leading to larger architectures. A straightforward MALDI protocol is introduced that significantly simplifies the analysis and characterization of the CPP-based noncovalent complexes with unprecedented selectivity and sensitivity and led to the discovery of new [ring $\supset$ fullerene]-complexes. Tandem mass spectrometry (MS<sup>2</sup>) was applied to establish the location of the charge on either the inner or outer moiety of the supramolecular host-guest systems. Competition experiments in which fullerenes and CPPs compete in complex formation revealed the most favorable combinations for noncovalent interaction. Density functional theory (DFT) was used to calculate geometries and binding energies as well as fragmentation energies of CPP $\supset$ fullerene complexes.

## Results and Discussion

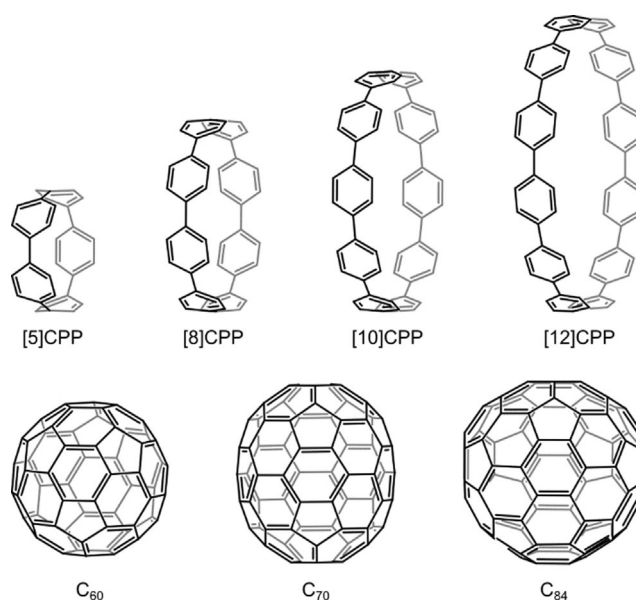
### Direct LDI of cycloparaphenylenes (CPPs)

The application of direct laser desorption/ionization (LDI) leads to a stunning result: all CPPs under investigation (Scheme 1) are not only abundantly transferred into the gas phase and ionized, but the respective radical cations are formed essentially without any sign of fragmentation. The positive-ion mode LDI mass spectra of the four CPPs are displayed in Figures 1a–d.

The ion formation is so efficient that molecular ions could be observed even at the highest laser attenuation possible with our equipment. The resulting radical cations resist secondary reactions up to fairly elevated laser fluences. This demonstrates both very efficient ion formation and considerable resilience towards fragmentation upon direct laser ablation. Hence, for the sensitive analysis of CPPs, it is not necessary to conduct the frequently found MALDI protocol involving the careful addition of a matrix with the intention to soften the supposed harshness of the direct LDI analysis.<sup>[1,8,9]</sup> The reason for the effi-

cient ionization during positive-ion mode LDI is twofold. On the one hand, CPPs feature a ring size independent strong absorption maximum<sup>[1,4]</sup> at the excitation wavelength of the employed N<sub>2</sub>-laser (337 nm, Figure 1e).<sup>[4]</sup> This guarantees the efficient photon absorption upon laser irradiation of the CPPs. On the other hand, CPPs possess relatively low ionization potentials.<sup>[52]</sup> In fact, the ionization of the CPPs studied here is accessible by the addition of two photons from the N<sub>2</sub>-laser, which makes it highly likely that the CPPs undergo ionization by a 2-photon-ionization process.<sup>[53]</sup>

At elevated laser fluences new signals emerge at higher masses. The corresponding ions are CPP oligomers (Figure 2a–d) and dedicated experiments (see below) reveal that these oligomers feature strong covalent bonding. The formation process shows thus similarities to the laser-induced coalescence of fullerenes<sup>[54]</sup> or the cross-linking of polyynes<sup>[40]</sup> rather than to the formation of weakly bound noncovalent aggregates held together by  $\pi$ – $\pi$ -stacking or dispersion forces, as observed for other electron-rich  $\pi$ -extended carbon systems.<sup>[42,55]</sup> Oligomeric CPP ions were observed for all ring sizes with signals corresponding to the radical cation of the CPP multimer and/or the ion lacking one hydrogen atom. [5]CPP displays the highest degree of oligomerization. Oligomers were observed up to the heptamer and the dimer was produced with the highest absolute intensity of all CPPs investigated. The dimer abundance is used here as an additional indicator for the extent of oligomerization and has been carefully measured for all CPPs using the same conditions. The increased reactivity of the [5]CPP ring may reasonably be caused by the strain energy,<sup>[8,9]</sup> which is largest for the smallest ring. [8]- and [10]CPP both show signals up to the tetramer. However, [8]CPP produced the oligomers more abundantly. This is particularly evident for the dimer formation, which was twice as abundant for [8]CPP. Again, this is in line with the assumption that the increased reactivity is



**Scheme 1.** Structures of utilized molecules. For C<sub>84</sub>, isomer 23 with D<sub>2d</sub>-symmetry is shown as example.<sup>[35]</sup>

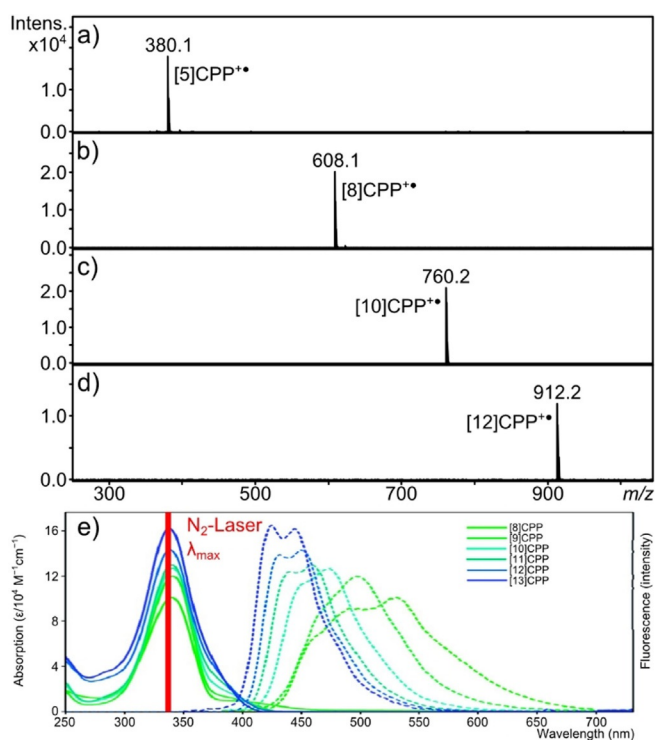


**Figure 1.** a)–d) LDI mass spectra of [5]-, [8]-, [10]-, and [12]CPP in the positive-ion mode, respectively. e) Absorption spectra of [8]-[13]CPP with the red line indicating  $\lambda_{\text{max}}$  of the  $\text{N}_2$ -laser. Adapted with permission from T. Iwamoto, Y. Watanabe, Y. Sakamoto, T. Suzuki, S. Yamago, *J. Am. Chem. Soc.* **2011**, *133*, 8354–8361. Reproduced with permission. Copyright 2011 American Chemical Society.<sup>[4]</sup>

caused by the higher strain energy of the smaller ring. [12]CPP affirms the trend of decreasing reactivity towards oligomerization with increasing ring size. The largest coalescence product is just the trimer and the dimer is formed with the lowest absolute intensity of all ring sizes.

In order to shed more light onto the mechanisms operative in the oligomerization process, mixed targets containing two different CPPs were laser ablated. A rough differentiation of the oligomerization process may distinguish a process in which cross linking occurs between intact CPP rings from an alternative mechanism involving ring opening to linear paraphenylenes (LPPs) prior to the intermolecular bond formation. The covalent linking of two intact CPP rings of different ring sizes is likely to be geometrically disfavored and/or to induce more strain compared to the dimerization of two rings of equal size. As a result, the formation of the two homodimers will be favored over the statistical formation of the heterodimer. In contrast, if ring opening would precede the dimerization, the resulting LPPs are likely to efficiently connect independent of the former CPP ring size, leading to a statistical distribution of homo- and heterodimers. The resulting pattern would be a 1:2:1 triplet with the mixed heterodimer being twice as abundant as the two homodimers. Figure 2e shows the LDI mass spectrum of a target obtained by drying a solution of equimolar amounts of [8]- and [12]CPP. The obtained dimer pattern resembles closely a triplet and is thus in line with a mechanism involving ring opening followed by LPP

cross linking rather than a ring-size dependent crosslinking of intact CPPs. However, this dimer pattern is not commonly observed. Other binary CPP combinations showed a different behavior. The target produced from a solution with equimolar content of [8]- and [10]CPP led to LDI mass spectra with three different appearances (Figure S3). Depending on the target area that was laser ablated, spectra were obtained with either [8]CPP<sub>2</sub> or [10]CPP<sub>2</sub> being more pronounced and spectra showing the mixed dimer with the most intense signal, displaying a similar pattern as observed in Figure 2e. We assume that the drying process of the mixed [8]CPP/[10]CPP solution created inhomogeneous target areas in which either the [8]CPP, the [10]CPP or the mixture crystallized more pronounced, which upon LDI led to the preferred formation of the respective dimers. This is also corroborated by the formation of either [8]CPP<sub>2</sub> or [10]CPP<sub>2</sub> without abundant observation of both dimers in one area. This observation is in line with the presence of “islands” of pure and mixed CPPs. For the mixed [8]CPP/[12]CPP solution we assume that both rings are capable of crystallizing more efficiently with each other, forming a homogeneous binary crystal structure over the entire area.

Following the idea of the ring-opening mechanism, we calculated the energy requirements for the CPPs under study. We contrasted a simple homolytic cleavage between two adjacent phenylene units, with a hypothetical ring opening involving a hydrogen rearrangement. The latter pathway would yield one terminal phenylene with a hydrogen at the position of the cleaved bond, while the other phenylene would adapt an aryne-like structure (for further details see section B in the Supporting Information). The resulting energies for the different ring opening mechanisms of CPP radical cations are listed in Table 1. In all cases, the rearrangement reaction, yielding the aryne, is energetically favored by more than 1 eV (23.06 kcal mol<sup>-1</sup>). It is interesting to note that the required dissociation energies correlate with the size and the strain energies of the CPPs. The smaller the ring, the larger the strain and therefore the smaller the energy required to obtain the LPP. Consequently, it is more likely for smaller rings to undergo ring-opening reactions under laser irradiation than for larger CPPs. As a result, the theoretical trend for the ring-opening energies would support the observed trend for the laser-induced oligomerization of the CPPs under study.

Negative-ion-mode LDI showed similarities to the positive-ion mode (Figure S2) in that signals for CPPs and their oligomers were found. However, there were also significant differences. First, the detection of any CPP-related signal was only possible at markedly increased laser power, indicating a less efficient ionization in the negative polarity. Second, the CPPs were not detected as radical anions, but as their deprotonated quasi-molecular anions  $[M-H]^-$ . Only in case of [5]CPP a molecular anion radical was observed, even more abundantly than the deprotonated species ( $I_{\text{rad}}/I_{\text{deprot.}} \approx 3.5:1$ ). This cannot be caused by differences in electron affinity (EA), since the EAs of the different CPPs are rather low and very similar.<sup>[52]</sup> However, electron uptake may lead to a considerable release of ring strain in [5]CPP, due to a more quinoidal-like structure of the LUMO in the anion compared to the benzenoid structure of

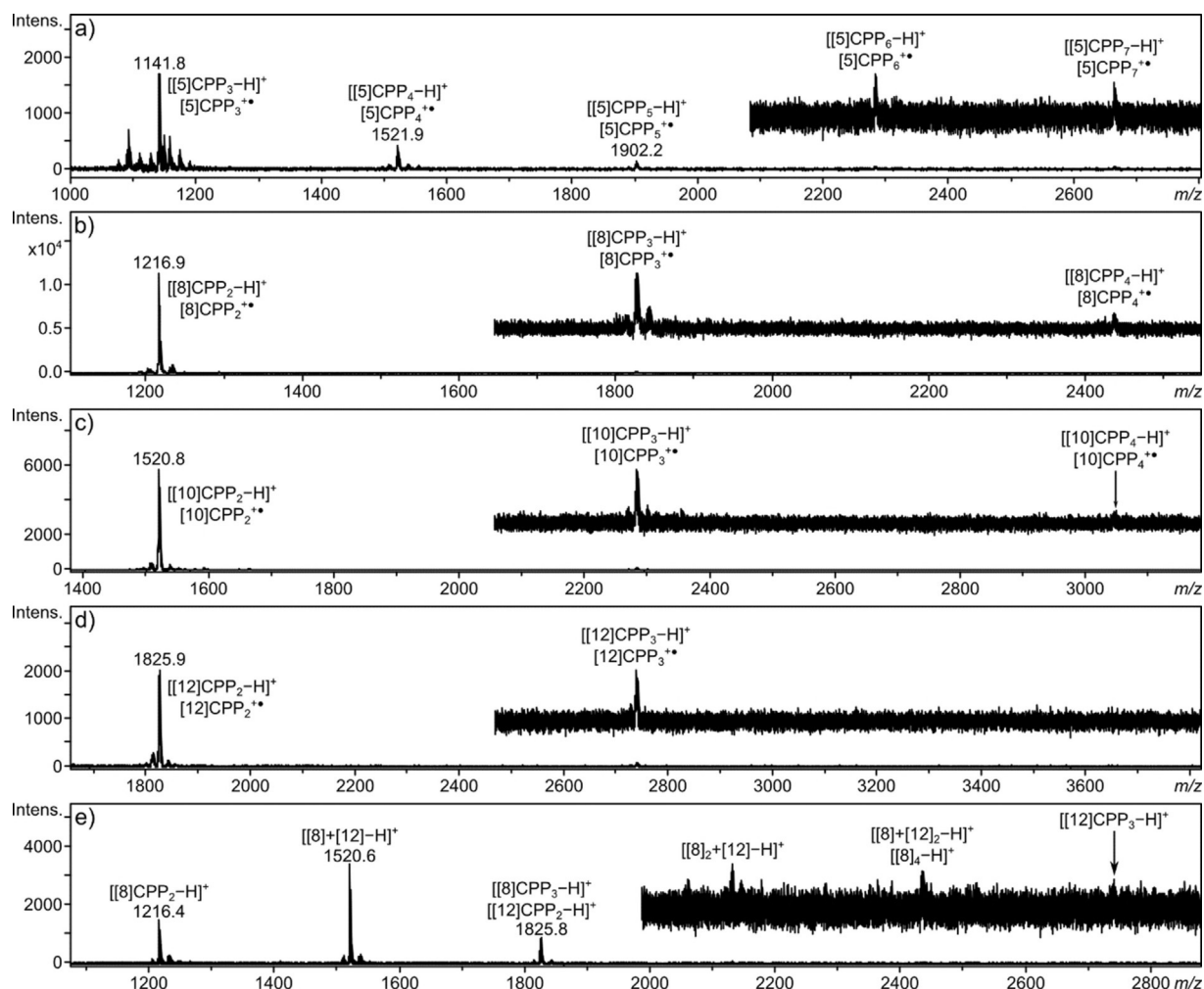


**Figure 2.** Positive-ion mode LDI mass spectra at elevated laser fluence of a) [5]CPP, b) [8]CPP, c) [10]CPP, d) [12]CPP, and e) an equimolar mixture of [8]- and [12]CPP.

the neutral,<sup>[8,9]</sup> Strain release by electron uptake would be a more relevant driving force for the [5]CPP ring compared to other ring sizes.

### Fragmentation of CPP and CPP-dimer ions

In order to gain insight into structure and type of binding within the observed multimeric CPP ions, daughter ion mass spectra were obtained. In these tandem mass spectrometry (MS<sup>2</sup>) experiments the fragment ions of a selected precursor

ion are recorded. The fragmentation pattern may reveal structural features of the dissociating precursor ion. The technical term for the daughter ion analysis performed with the applied time-of-flight set up is post-source decay (PSD). The molecular CPP ions and their respective dimer ions were chosen as precursor ions for PSD. Larger ions were too low abundant to record PSD spectra. As an example, Figure 3 shows the PSD spectra of the [10]CPP monomer and dimer ion. For the other ring sizes the corresponding spectra can be found in the supplementary information (Figures S4 & S5). The fragmentation pattern of the CPP molecular ions (monomer) is reminiscent of the decay behavior known for polycyclic aromatic hydrocarbons (PAHs).<sup>[56,57]</sup> This is true for the pattern in which adjacent fragment ion signals are spaced by one CH<sub>x</sub> moiety and which is most likely caused by the loss of (CH<sub>x</sub>)<sub>n</sub> moieties from the molecular ion. However, unusual for a PAH structure is the observation that every sixth and seventh CH<sub>x</sub> loss is clearly pronounced. This may indicate that after the loss of either six or seven CH<sub>x</sub>-units, the remaining fragment ion can have an intact, energetically favorable six- or five-membered ring, respectively. The loss of a neutral fragment containing six or

**Table 1.** Calculated energies in eV (kcal mol<sup>-1</sup>) required for ring opening of CPP radical cations. Values were obtained on the B3LYP-D3/def2-TZVP level of theory.

[n]CPP	Homolytic bond cleavage	Aryne rearrangement
[5]	1.01 (23.32)	-0.03 (-0.77)
[8]	2.29 (52.75)	1.22 (28.12)
[10]	2.75 (63.35)	1.69 (38.99)
[12]	3.13 (72.08)	2.03 (46.71)

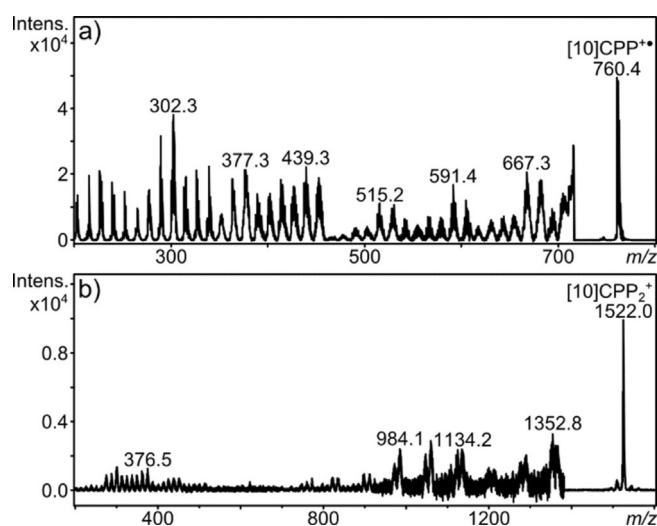


Figure 3. Post-source decay mass spectra of a) [10]CPP<sup>2+</sup> and b) [10]CPP<sub>2</sub><sup>2+</sup>.

seven carbon atoms makes it also likely, that the process is accompanied by ring opening. For a ring-opened benzoid CPP ion, the loss of C<sub>6</sub>H<sub>4</sub> units should be much more prominent, so that isomerization into quinoid structures seems a likely arrangement. However, conclusive structural insight remains minute based on the dissociation behavior. It should be emphasized that both the CPP radical cation and the CPP dication retain their ring structure upon oxidation of the neutral.<sup>[58]</sup> Ring opening would be the result of further activation.

The fragmentation behavior of the dimer radical cation shows exactly the same features as the monomeric radical cation, implying that the dissociation of both would proceed via similar structural motifs. Another indicative observation concerns the fact that the dimer ion does not show any signs of fragmentation back into the monomer cation. In a noncovalently bound dimer the two monomer units would be connected by the weakest bond. Thus, a noncovalent dimer would readily fragment back into one neutral and one charged monomer unit. The fact that such a dissociation is entirely absent is an indication of strong covalent bonding between the two CPP entities. This implies that a sort of covalent cross-linking has taken place between the units, similar to the recently described cross-linking between the acetylene groups in polyynes.<sup>[40]</sup>

### Ring-in-ring complexes in MALDI

Next, the investigation of noncovalent ring-in-ring host-guest complexes is outlined. First Fomine et al. then Bachrach et al. reported in theoretical studies on the stability of noncovalent CPP host-guest systems, referring to them as “Russian Doll”-like structures and “Planetary Orbit”, respectively.<sup>[15,16]</sup> They found that particular stable ring-in-ring complexes would result when the inner and the outer ring differ exactly by five phenylene units. Recently, Yamago and co-workers reported the first experimental proof of such complexes in solution by NMR and even found a ternary complex consisting of [15]CPP,

[10]CPP, and C<sub>60</sub>.<sup>[17]</sup> In the following MALDI mass spectrometry is demonstrated as an efficient method to investigate CPP ring-in-ring host-guest complexes by intact transfer into the gas phase accompanied by ionization. For proof of concept, the two CPPs were chosen that would fulfil the requirement of differing by five phenylene units, that is, [5]- and [10]CPP. Due to partial oxidation of the [5]CPP sample, we added this ring size in excess. Furthermore, DCTB as an electron transfer matrix was added to the target in a 500-fold excess with respect to [10]CPP. The resulting positive-ion mass spectrum is depicted in Figure 4a. The radical cations of both ring sizes are detected in the spectrum. The tremendous abundance of [5]CPP<sup>•+</sup> is mainly due to its use in excess to [10]CPP. In addition to the CPP<sup>•+</sup> signals the radical cation of the host-guest complex [[10]CPP⊃[5]CPP]<sup>•+</sup> is observed. The intensity of the complex is 24.3 % relative to the signal of [10]CPP<sup>•+</sup>. The abundant formation of the complex ion is remarkable in light of the fact that theory predicts that interaction energies within the ring-in-ring CPP host-guest complexes increase with pairs of increasing ring sizes, leaving [10]CPP⊃[5]CPP as the system with the weakest interaction energy.<sup>[15–17]</sup> The strength of the MALDI approach for the detection and characterization of ring-in-ring complexes becomes particularly obvious when considering that a strong solitary signal is obtained in addition to a characteristic isotope pattern, compared to the NMR detection relying on a minute shift of 0.002 ppm between free and complexed [5]CPP.<sup>[17]</sup>

All efforts failed to detect the [10]CPP⊃[5]CPP complex intact in the harsh LDI experiment that is, without the DCTB matrix, which underlines that the use of the matrix is essential in this case. Moreover, MALDI applied to a mixture of [8]- and [12]CPP (Figure S6) did not show the ring-in-ring complex. Clearly, the expected weaker interaction between two rings differing by only four phenylene units is not strong enough to survive the MALDI experiment. Based on the present findings, it is proposed that solvent-free MALDI,<sup>[30]</sup> a variant of the method that avoids the use of a solvent, should be able to achieve the detection of complexes with larger CPPs, which escaped the analysis by NMR due to precipitation.<sup>[17]</sup>

Figure 4b displays the PSD daughter ion mass spectrum of the [[10]CPP⊃[5]CPP]<sup>•+</sup> precursor ion. The ion features only one fragmentation pathway, that is, the loss of the outer [10]CPP ring as a neutral species while the charge resides on the inner [5]CPP ring. This dissociation experiment thus reveals the charge distribution in the cationic noncovalent complex ion. The observed charge distribution, with the radical cation located on the inner ring and the outer ring being a neutral, was theoretically predicted by Fomine et al.<sup>[15]</sup> They argued that the charge residing on the smaller ring is due to differences in the ionization potentials. For [5]- and [10]CPP, however, the difference in their ionization potential is just 0.05 eV (1.15 kcal mol<sup>-1</sup>)<sup>[52]</sup> which makes it rather unlikely that the preference of the charge for the inner ring is so undivided, so that [10]CPP<sup>•+</sup> should be detected as well. Yamago and co-workers calculated the frontier orbitals of ring-in-ring complexes and found that the HOMO of each host-guest complex is exclusively located on the inner CPP.<sup>[17]</sup> Therefore, we assume that in

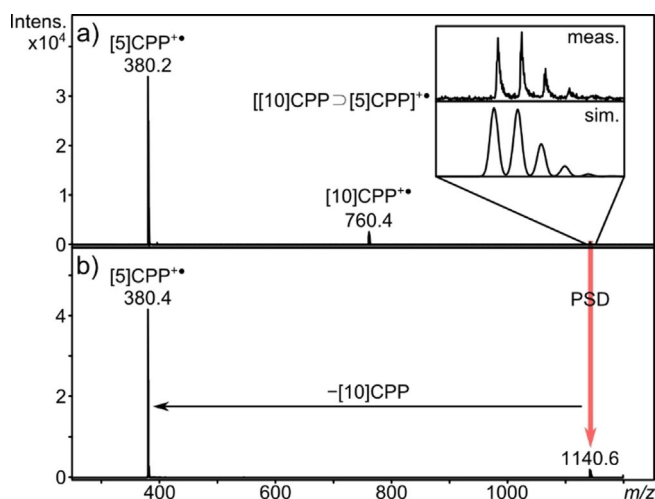


**Figure 4.** a) MALDI mass spectrum of a [5]- and [10]CPP mixture. The inset shows the signal of the ring-in-ring inclusion complex with its simulated isotope pattern below. b) PSD mass spectrum of  $[[10]CPP\supset[5]CPP]^{+\bullet}$  with the charge remaining on the [5]CPP, and [10]CPP being lost as a neutral.

the MALDI experiment the electron transfer to the matrix occurred from the HOMO of the complex, ionizing the inner ring and leaving the host CPP uncharged.

#### CPP⊃fullerene host–guest complexes in MALDI

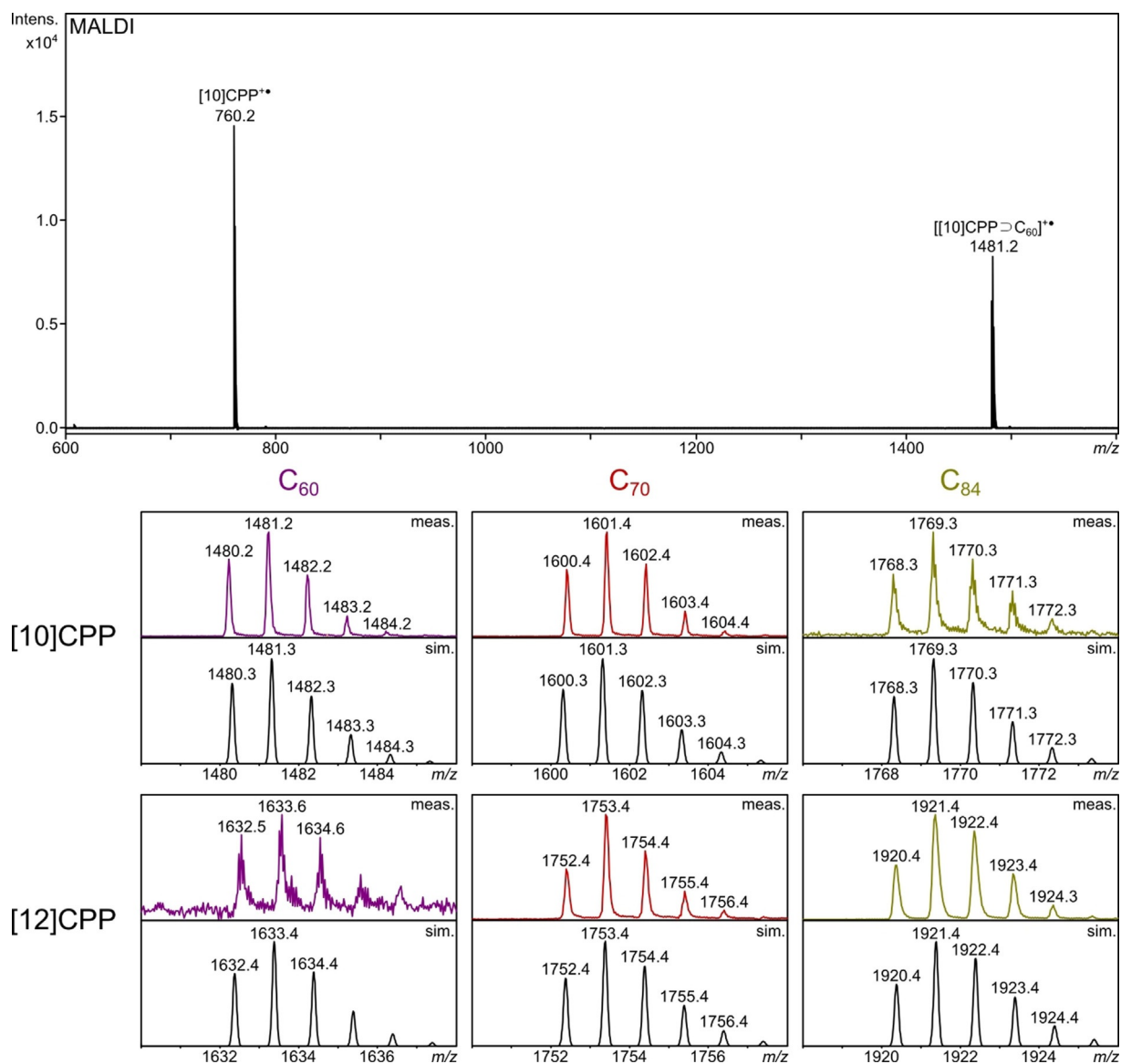
In the following the performance of MALDI is evaluated as a means to detect and characterize host–guest complexes of fullerenes (guest) and CPPs (host). The target mixture was composed of a chosen fullerene with either [10]- or [12]CPP in an equimolar ratio and DCTB as the matrix in 500-fold excess. The proof-of-concept experiment was conducted with  $[10]CPP\supset C_{60}$  as the first ever observed complex<sup>[23]</sup> and, therefore, one of the best studied CPP–fullerene systems. The top trace in Figure 5 displays the resulting positive-ion mode MALDI-ToF mass spectrum. The spectrum is dominated by the signal of the radical cation,  $[10]CPP^{+\bullet}$ , while the corresponding signal of  $C_{60}^{+\bullet}$  is entirely absent. Because of its lower ionization energy,  $C_{60}$  is likely to be ionized in reaction with the DCTB radical cation, which is one of the primary ions derived from the matrix. However, the ionization of the CPPs requires even lower energies than of fullerenes, so that the radical cation formation of  $C_{60}$  is not likely to compete with the formation of  $CPP^{+\bullet}$ . The most striking feature, however, represents the second most abundant signal of the desired host–guest complex,  $[10]CPP\supset C_{60}^{+\bullet}$  (80.3% compared to  $[10]CPP^{+\bullet}$ ). This finding provides clear evidence of the suitability of MALDI as a sensitive analytical tool for the formation of noncovalent CPP⊃fullerene complexes.

In order to prove that the [60]fullerene is definitely located inside the CPP ring we conducted a control experiment, replacing [10]CPP by [8]CPP. The cavity of the [8]CPP ring is too small for  $C_{60}$  to reside inside, resulting in a hovering of the fullerene above the center of the nanohoop.<sup>[20]</sup> As a result of the considerably weaker bonding it is highly questionable that MALDI would still be able to produce a signal of the undissociated complex. In Figure S7 the resulting mass spectrum is shown.

The only signal observed was caused by the radical cation of [8]CPP, in turn providing strong evidence that  $[[10]CPP\supset C_{60}]^{+\bullet}$  is indeed an inclusion complex.

Next, different combinations of nanohoops and fullerenes were combined. For [10]CPP (Figure 5 bottom part upper half) complexation with  $C_{70}$  (12.2% relative to  $[10]CPP^{+\bullet}$ ) was achieved as well. This host–guest system was already observed by Yamago and co-workers by NMR spectroscopy in solution<sup>[25]</sup> and now for the first time it was successfully transferred into the gas phase and ionized. It was even possible to generate the noncovalent complex of [10]CPP with  $C_{84}$ . The [84]fullerene has a larger diameter than the fullerenes previously investigated, which makes it sterically more demanding for it to fit into the [10]CPP. In fact, our computational analysis (see below for Computational Results) shows that the most frequent  $C_{84}$  ( $D_{2d}$  isomer 23) isomer would not be able to fit into the ring. However, a  $D_2$  isomer (isomer 22) would fit upon insertion in a standing position. The resulting complex cannot achieve the ideal interlayer distance between the nanohoop and the fullerenes of 3.3–3.5 nm so that attractive interactions are expected to be less pronounced. Nevertheless, we were able to generate  $[[10]CPP\supset C_{84}]^{+\bullet}$  (0.25%) in MALDI. Although the relative intensity was only low, the well resolved isotope pattern identifies the complex as a stable species. This host–guest system is observed here for the first time, featuring the largest buckyball so far encapsulated by [10]CPP. However, our  $C_{84}$  sample is a mixture of isomers (see Experimental section), not allowing a distinction by the mass spectrum.

The fullerene complexation with [12]CPP gained only little attention in the literature. A theoretical study has examined  $[12]CPP\supset C_{70}$ <sup>[19]</sup> which was also studied experimentally by Raman spectroscopy.<sup>[59]</sup> The latter study found only minor changes in the Raman bands upon complexation, making it difficult to study the formation of the host–guest system. Since [12]CPP has a larger ring size than [10]CPP, it is tempting to commence with  $C_{84}$  in order to see whether the encapsulation is more efficient. Positive-ion mode MALDI delivered the desired host–guest system  $[[12]CPP\supset C_{84}]^{+\bullet}$  in an abundance of 10% relative to the radical cation of [12]CPP. The complex-to-CPP ratio in the MALDI experiment is thus 40 times larger than with [10]CPP. The complex with the next smaller stable fullerene,  $[12]CPP\supset C_{70}$ , was calculated to have a rather low binding energy compared to the complex with  $[10]CPP$ <sup>[19]</sup> and in fact, remained undetected by NMR spectroscopy.<sup>[25]</sup> In the present experiments  $[12]CPP\supset C_{70}^{+\bullet}$  was observed with good intensity (6.5% of free  $CPP^{+\bullet}$ ) and matching isotope pattern. The complex-to-CPP ratio is half the value obtained with [10]CPP (12.2%), in line with a lower binding energy in  $[12]CPP\supset C_{70}^{+\bullet}$ . Even for  $C_{60}$ , which has the smallest possible area for attractive interactions with [12]CPP, a signal for the host–guest complex was obtained (0.44% of free  $CPP^{+\bullet}$ ), in good agreement with the simulated isotope pattern. The observation of this labile complex, once again establishes MALDI as a powerful tool for the sensitive analysis of fullerene–CPP aggregates, in particular when considering that this host–guest pair was not detected in NMR/solution experiments.<sup>[23]</sup>



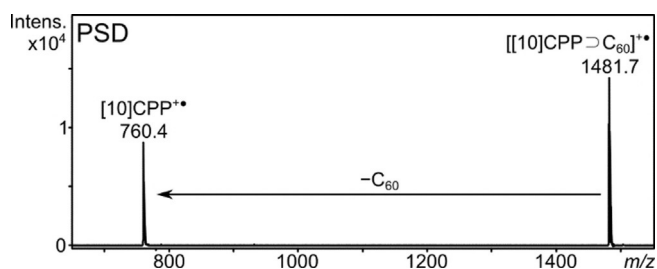
**Figure 5.** Top: MALDI mass spectrum of a [10]CPP, C<sub>60</sub> mixture displaying the host–guest complex. Bottom: enlarged spectral regions of the various [CPP>fullerene]<sup>••</sup> complexes with their respective simulated spectra below.

Figure 6 displays the PSD daughter ion spectrum of [[10]CPP>C<sub>60</sub>]<sup>••</sup> which reveals the charge distribution of the dissociating complex. Unlike the ring-in-ring aggregate (compare PSD spectrum in Figure 4b)), we observed that charge of the fullerene-in-ring complex remains at the outer species so that no signal of the C<sub>60</sub> radical cation is produced in the dissociation. A rationale for the observed charge distribution has to be seen on the one hand, in the fact that the ionization potential of the C<sub>60</sub> is considerably larger than the one of [10]CPP (7.57 eV (174.56 kcal mol<sup>-1</sup>) compared to 6.39 eV (147.35 kcal mol<sup>-1</sup>), respectively).<sup>[52,60]</sup> Therefore, the charge residing on the ring is thermodynamically more favorable than being on the fullerene. On the other hand, frontier orbital calculations of the neutral complex, as performed by Rio et al. and by Zhao and co-workers, indicate that the HOMO of the complex is exclusively located on the CPP.<sup>[20,22]</sup> Therefore, assuming that upon ionization the electron is released from the HOMO of

the host–guest system, as it was already reasoned for [[10]CPP>[5]CPP]<sup>••</sup>.

The next set of MALDI experiments explores the possibility of selective binding between nano hoops and fullerenes when two CPPs compete for a given fullerene. Hence, equimolar mixtures of [10]-, [12]CPP, and either C<sub>60</sub>, C<sub>70</sub> or C<sub>84</sub> were mixed together with an excess amount of the DCTB matrix (500-fold). The resulting spectra are displayed in Figure 7. The three targets show significant variations in the resulting product ion distributions. For the C<sub>60</sub>-containing target (Figure 7a), the radical cations of both CPP rings are observed, with the signal of free, uncomplexed [12]CPP<sup>••</sup> being notably more intense than the one for [10]CPP<sup>••</sup>. This may already be taken as an indication that free [12]CPP is more abundantly present in the target, due to the more efficient complexation of [10]CPP with the fullerene. Inspecting the region of the spectrum that contains the signals of possible complexes confirms the assump-





**Figure 6.** PSD mass spectrum of  $[[10]\text{CPP}\supset\text{C}_{60}]^{+\bullet}$  displaying the loss of the fullerene with the charge localized on the CPP.

tion. The only host–guest system detected is  $[[10]\text{CPP}\supset\text{C}_{60}]^{+\bullet}$  while  $[[12]\text{CPP}\supset\text{C}_{60}]^{+\bullet}$  is essentially absent, revealing selective binding of  $\text{C}_{60}$  to [10]CPP with respect to [12]CPP. Switching to  $\text{C}_{70}$  changes this preference (Figure 7b). The radical cations of both free CPP rings are now almost equal in intensity, which might be an indication for unselective binding to  $\text{C}_{70}$ . The detected complexes affirm this assumption, as the host–guest systems are also observed in almost equal abundances. This observation is remarkable, because NMR studies in solution showed selective binding of  $\text{C}_{70}$  just to [10]- and [11]CPP, and not at all to [12]CPP.<sup>[25]</sup> A possible explanation for the conflicting findings obtained by NMR and MALDI might be due to the

possibility that the complex formation with [12]CPP may occur during the drying process of the MALDI sample preparation. Therefore,  $[[12]\text{CPP}\supset\text{C}_{70}]^{+\bullet}$  may not be formed in solution, but during the evaporation of the solvent yielding the complex in the solid-state. Finally,  $\text{C}_{84}$  induces yet another product ion distribution. Free [12]CPP is less abundant than [10]CPP suggesting a reversed selectivity as was observed for  $\text{C}_{60}$ . The complex detected in this MALDI experiment was exclusively  $[[12]\text{CPP}\supset\text{C}_{84}]^{+\bullet}$  with no signal for the complex with [10]CPP, providing proof for the selective binding of  $\text{C}_{84}$  to [12]CPP.

Changing the competition experiment so that two fullerene guest molecules would compete for one nanohoop host confirms these findings, exhibiting the same tendencies of selective binding. When  $\text{C}_{60}$  and  $\text{C}_{70}$  compete for the binding site of [12]CPP (Figure S8a), the most intense signal is caused by the radical cation of [12]CPP, while signals of the two fullerenes are entirely absent. Selective complex formation is evident, since  $[[12]\text{CPP}\supset\text{C}_{70}]^{+\bullet}$  is the only noncovalent complex observed. Once again this confirms that the preferred interaction of fullerene and nanohoop can result in selective binding. If  $\text{C}_{60}$  is replaced by  $\text{C}_{84}$ , selective binding is not observed, because both fullerenes interact comparatively well with the nanohoop (Figure S8b).

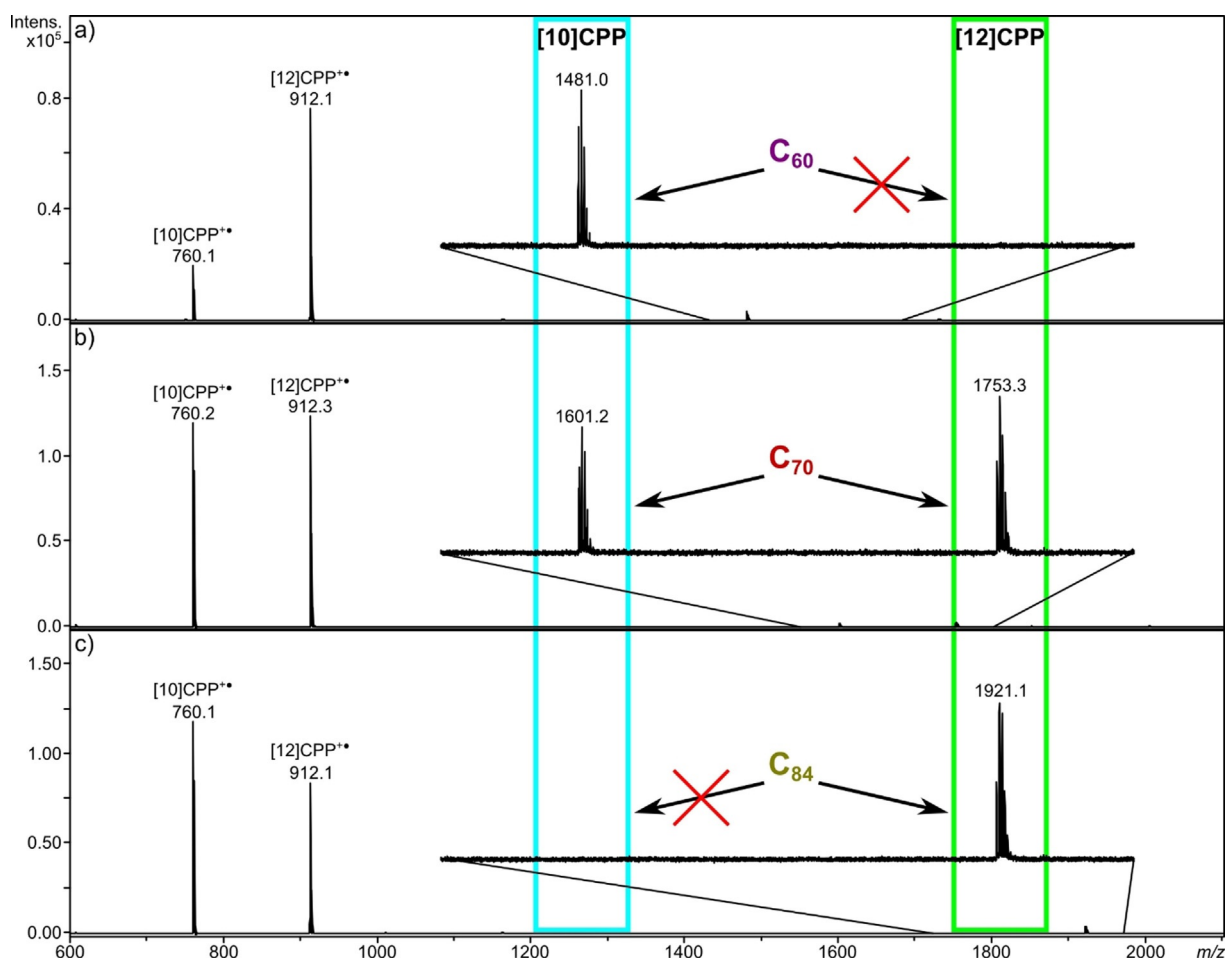


**Figure 7.** Selective fullerene binding experiments to [10]- and [12]CPP with a)  $\text{C}_{60}$ , b)  $\text{C}_{70}$ , or c)  $\text{C}_{84}$ .

Both outlined competition experiments above reveal clearly that complex formation depends essentially on the convex-concave  $\pi$ - $\pi$ -interaction between fullerene and CPP ring. While  $C_{60}$  forms with [10]CPP efficiently a complex, the complex formation with the larger [12]CPP ring is so inefficient that no complex is observed. For  $C_{70}$  both ring sizes of [10]- and [12]CPP are attractive and complexes are abundantly formed. Here the complexation remains unselective. For  $C_{84}$ , however, complex formation occurs selectively with the [12]CPP ring, while interaction with the narrower [10]CPP ring cannot compete. The most prominent isomer of  $C_{84}$  ( $D_{2d}$ ) does not fit into [10]CPP, however the  $D_2$  isomer does in standing orientation (see section Computational Results).  $C_{70}$  and  $C_{84}$  are both attractive guests for the [12]CPP host in the MALDI experiment. The two complexes that were not observed in the competition experiments; that is, [12]CPP $\supset$  $C_{60}$  and [10]CPP $\supset$  $C_{84}$ , are perfectly stable noncovalent complexes, but were just not formed because of more attractive combinations accessible in the competition experiment. The selective binding of fullerenes by CPPs might help extracting a desired fullerene from raw soot, resulting in an improved separation process for fullerenes, as was already shown by Shinohara and co-workers for endohedral fullerenes.<sup>[28]</sup> The MALDI analysis in the negative-ion mode needed higher laser fluences and gave less reliable data.

## Computational Results

All calculation results discussed in this section were obtained at the B3LYP-D3 level of theory (see calculation settings for details). For the investigated  $[n]$ CPP $\supset$ fullerene complexes the formation energies have been calculated as energy difference of the energy of the CPP $\supset$ fullerene complex minus the sum of energies of the CPP and the fullerene forming it. For a given CPP $\supset$ fullerene complex typically several conformations representing local minima on the potential energy surface have been found.

Table 2 lists formation and fragmentation energies for the most stable conformer. Data for other conformers can be found in Table T6 and T7, Supporting Information. Fragmentation energies have been calculated as the sum of the energies of the positively charged CPP $^{+}$  and the fullerene minus the CPP $\supset$ fullerene $^{+}$  energies, see Table 2. Fragmentations leading to a positively charged fullerene instead of a CPP $^{+}$  cation exhibit a much higher fragmentation energy, see Tables T8–T12, Supporting Information.

Geometry optimization of [8]CPP $\supset$  $C_{60}$  reveals that the neutral [8]CPP is too small to act as a host for  $C_{60}$  fullerene. As a result, the fullerene hovers above the center of the CPP ring and displays vdW interactions with just the edge of the CPP (Figure 8). Thus [8]CPP $\supset$  $C_{60}$  complexes are energetically not as attractive as [10]CPP $\supset$  $C_{60}$  complexes and less stable. Accordingly, these could not be detected in our MALDI experiments (see above).

The magnitude of the formation energy is highest for [10]CPP $\supset$  $C_{70}$  with the fullerene in standing orientation. Of the two main isomers of  $C_{84}$ , only  $C_{84}$  ( $D_2$ ) can be encapsulated by

[10]CPP, while  $C_{84}$  ( $D_{2d}$ ) does not fit into the nanohoop (Figure 8). The formation energy of [10]CPP $\supset$  $C_{84}$ ( $D_2$ ) is lower compared to [10]CPP $\supset$  $C_{70}$ . This is caused by the increased strain in the [10]CPP as a much tighter belt around the  $C_{84}$  (Table 2). The oval-shaped  $C_{84}$  ( $D_2$ ) fits into the CPP in a standing orientation, with the [10]CPP cavity being large enough to fit around the small circumference of  $C_{84}$  ( $D_2$ ). During the optimization, the ring does not move towards the bottom or the top of the fullerene. For the [10]CPP $\supset$  $C_{84}$  complex of the  $D_{2d}$  isomer a geometry similar to the [8]CPP $\supset$  $C_{60}$  was obtained. The spherical  $C_{84}$  ( $D_{2d}$ ) is too large for the [10]CPP to form an inclusion complex, therefore, the fullerene is loosely bound to the CPP and hovers above it (Figure 8b). This selective complexation of  $C_{84}$  isomers indicates that [10]CPP might be a promising tool for the preparation of isomerically pure  $C_{84}$  samples.

Turning to the bigger [12]CPP ring, the formation energies of the [12]CPP $\supset$ fullerene complexes increase with the size of the encapsulated fullerene. The smaller fullerenes  $C_{60}$  and  $C_{70}$  can only interact partially with the CPP ring, whereas the larger  $C_{84}$  exhibits interactions with the entire CPP ring (Table 2, Figure 8c). The highest formation energy is obtained for the oval  $C_{84}$  ( $D_2$ ) in lying orientation, as it has the larger interaction area compared to the more spherical  $C_{84}$  ( $D_{2d}$ ) (Figure 8c). The positively charged complexes do not show significant differences in their geometries, with the CPP remaining around the middle of the fullerene to maximize the interaction area as no size conflicts occur for the large [12]CPP. Figure 8c) shows the vdW interaction areas for the [12]CPP $\supset$  $C_{60}$  and [12]CPP $\supset$  $C_{84}$  complexes. The vdW interaction area covers about half of the CPP for  $C_{60}$ , whereas for  $C_{84}$  vdW interactions are present for the whole CPP ring. If larger fullerenes are hosted inside the CPPs, the phenylene units of the CPPs are less twisted against each other in order to optimize the geometry for maximal vdW interactions.

For the calculation of the [[10]CPP $\supset$ [5]CPP] ring-in-ring complex we focused on the “Russian doll” conformation as it is reported to be the most stable conformation.<sup>[17]</sup> A formation energy of 1.55 eV (35.74 kcal mol $^{-1}$ ) was obtained for the neutral complex, which is lower compared to the formation energies of the most stable CPP $\supset$ fullerene complexes in this work. Fragmentation energies of the [[10]CPP $\supset$ [5]CPP] $^{+}$  are lower if

**Table 2.** Calculated binding and fragmentation energies in eV (kcal mol $^{-1}$ ) of various CPP $\supset$ fullerene complexes on the B3LYP-D3 def2-TZVP level of theory. Fragmentation energies are listed for the fragmentation leading to a CPP cation.

Fullerene	[10]CPP $\supset$ $C_n$ $E_{\text{bind}}$	[10]CPP $\supset$ $C_n^{+}$ $-E_{\text{frag}}$	[12]CPP $\supset$ $C_n$ $E_{\text{bind}}$	[12]CPP $\supset$ $C_n^{+}$ $-E_{\text{frag}}$
$C_{60}$	-2.01 (-46.35)	-1.95 (-44.97)	-1.21 (-27.90)	-1.20 (-27.67)
$C_{70}$	-2.11 (-48.66)	-2.08 (-47.97)	-1.40 (-32.28)	-1.39 (-32.05)
$C_{84}$ ( $D_{2d}$ )	-1.55 (-35.74)	-1.55 (-35.74)	-1.77 (-40.81)	-1.72 (-39.66)
$C_{84}$ ( $D_2$ )	-1.89 (-43.58)	-1.92 (-44.28)	-2.00 (-46.12)	-2.01 (-46.35)

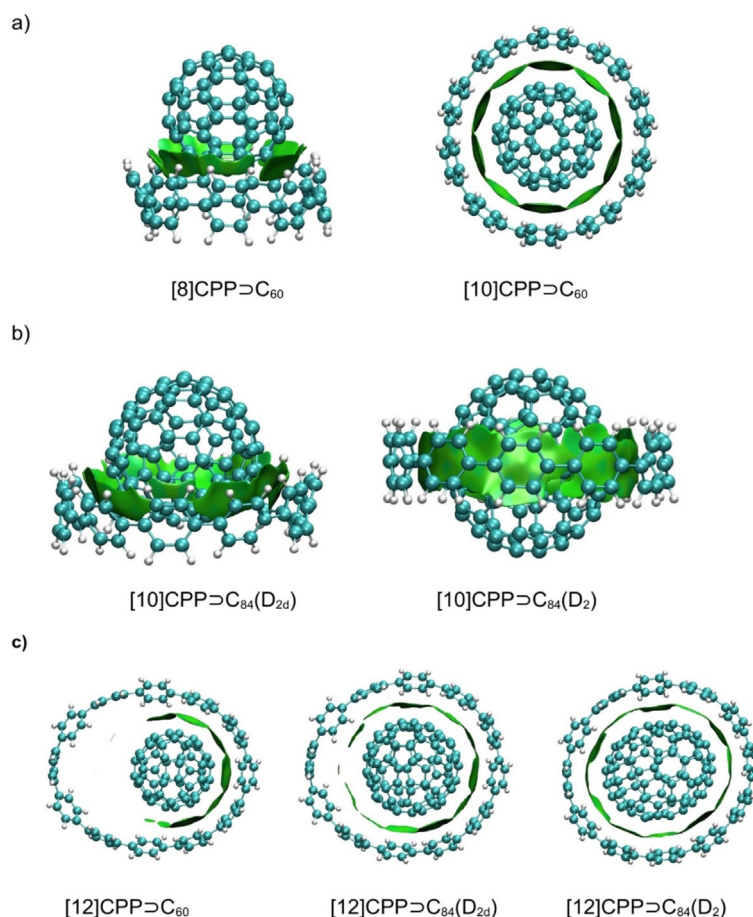


**Figure 8.** Calculated structures for various neutral CPP⊃fullerene complexes obtained on the B3LYP def2-TZVP level of theory. a) Complexes of [8]CPP and [10]CPP with C<sub>60</sub>. b) [10]CPP complexes with C<sub>84</sub> fullerenes. On the left the D<sub>2d</sub> on the right the D<sub>2</sub> isomer. c) [12]CPP with C<sub>60</sub> (left), C<sub>84</sub> (D<sub>2d</sub>) (middle), and C<sub>84</sub> (D<sub>2</sub>) (right).

the charge resides on [5]CPP (1.99 eV (45.89 kcal mol<sup>-1</sup>)) instead of [10]CPP (2.12 eV (48.89 kcal mol<sup>-1</sup>)), which is in line with the HOMO of the ring-in-ring complex being located on the smaller ring.<sup>[17]</sup>

## Conclusions

In summary, [5]- to [12]CPP rings can be readily transferred into the gas phase and ionized by direct LDI without decomposition. The ring-size independent absorption maximum at the N<sub>2</sub>-laser wavelength facilitates the process. Increasing the laser power results in coalescence most probably involving ring opening followed by cross linking. Fragmentation of monomers and dimers display similar fragmentation behaviors indicating strong covalent bonding of oligomers. The radical cation of the ring-in-ring complex of [5]- and [10]CPP was generated by MALDI and -upon excitation- fragmented by loss of the neutral [10]CPP, indicating that the electron was removed from the HOMO of the complex, that resides on the [5]CPP. Additionally, MALDI was introduced as a new sensitive method to identify and characterize CPP⊃fullerene host-guest complexes, also enabling the detection of several complexes so far unknown in literature. The MALDI method described herein may

therefore be useful for researchers aiming to develop purification protocols for exotic fullerenes. Fragmentation of [[10]CPP⊃C<sub>60</sub>]<sup>++</sup> resulted in the CPP<sup>++</sup> being the only fragmentation ion. Again, the electron was most likely extracted from the HOMO of the complex, which is located on the outer CPP. Selective binding can be achieved, if two CPPs compete for one fullerene or vice versa two fullerenes compete for one CPP ring, depending on the most favorable vdW interactions within the inclusion complexes.

## Experimental Section

**Chemicals:** [5]- and [12]CPP were purchased from TCI (Belgium) and used as supplied. [8]- and [10]CPP were synthesized according to previously reported procedures.<sup>[37]</sup> Dichloromethane (DCM) and toluene were purchased from VWR (Belgium, HPLC grade) and used without further purification. C<sub>84</sub> was purchased from Sigma-Aldrich. The supplier identifies the D<sub>2</sub> and D<sub>2d</sub> isomers as the two most prominent components.

**Sample preparation:** CPP stock solutions in DCM (0.2–0.3 g L<sup>-1</sup>) were prepared. For LDI experiments 1–3 μL of the stock solutions were pipetted onto the target and dried under ambient conditions. If more than one CPP was required, an equimolar mixture of the

given CPPs was prepared and put on the target as described above. In case of [5]CPP the exact concentration could not be obtained due to partial oxidation of the sample. For MALDI experiments *trans*-2-[3-(4-*tert*-butylphenyl)-2-methyl-2-propenylidene]malononitrile (DCTB, 10 g L<sup>-1</sup> in DCM) was used as matrix. The stock solutions of the fullerenes were prepared in toluene (0.2–1.0 g L<sup>-1</sup>) and sonicated until they were completely dissolved. C<sub>84</sub> tended to aggregate over time in toluene, thus the corresponding stock solutions were sonicated prior to every use. Ring-opening as well as the CPP-fullerene complexes were prepared by mixing the two respective molecules with the matrix in a 1:1:500 ratio. For the selective binding the molecules were mixed also in an equimolar ratio and matrix was added in a 500-fold excess. The sample solutions were dropped on the target (1–3 μL) and the solvent was evaporated under ambient conditions.

**Instrumentation:** As target a ground steel microtiter plate (MTP 384, Bruker, Bremen, Germany) was used. The (MA)LDI-ToF mass spectrometer was a Reflex IV (Bruker, Bremen, Germany) equipped with a nitrogen-laser (N<sub>2</sub>-laser, λ<sub>max</sub> = 337 nm) as used in several (MA)LDI studies before.<sup>[39,40]</sup> Spectra were recorded in the reflectron mode, the instrument is equipped with a linear-field reflectron. For tandem mass spectrometry (MS<sup>2</sup>), post-source decay (PSD) spectra were obtained as described in detail elsewhere.<sup>[41]</sup> Calibration of the mass scale was achieved with a polyethylene glycol polymer mix in the positive-ion mode and with (CsI)<sub>x</sub><sup>+</sup> clusters generated from CsI<sub>3</sub> in the negative-ion mode. Moreover, a poly-phenyl-porphyrin mixture was used as described in detail elsewhere.<sup>[42]</sup>

**Calculation settings:** Density-functional calculations have been performed using the TURBOMOLE software package (Version 7.1).<sup>[43]</sup> Geometries were optimized utilizing the PBE<sup>[44]</sup> and B3LYP<sup>[45,46]</sup> functional and def2-TZVP basis sets.<sup>[47]</sup> To increase the calculation speed the RI and MARIJ approximations were employed.<sup>[48]</sup> Dispersion effects were taken into account by using the Grimme D3 correction<sup>[49]</sup> with and without Becke-Johnson (BJ) damping.<sup>[50]</sup> Results for the B3LYP functional in conjunction with the D3 dispersion correction (B3LYP-D3) are shown and discussed later. Results for the PBE functional with D3 and D3BJ dispersion correction and for the B3LYP functional with D3 dispersion correction employing BJ damping (B3LYP-D3BJ) can be found in the Supporting Information. All computational settings lead to results that are qualitatively very similar. The magnitude in binding and fragmentation energies is increasing in the order PBE-D3 < B3LYP-D3 < B3LYP-D3BJ. The binding energies calculated in ref. [21] agree well with those calculated here.

In order to visualize intermolecular van der Waals (vdW) interactions contour plots of the reduced density gradient (RDG) were calculated and visualized at low electron density ρ, that is, electron densities below a certain threshold. [Eq. (1)]

$$RDG = \frac{1}{2(3\pi^2)^{1/3}} \frac{|\nabla\rho|}{\rho^{4/3}}$$

To identify attractive interactions  $sign(\lambda_2)\rho$  was evaluated with λ<sub>2</sub> being the second largest eigenvalue of the electron density Hessian matrix. These calculations were performed with the program NCIPLOT (Version 3.0) with a threshold for the density of ρ = 0.2 au.<sup>[51]</sup> The RDGs including noncovalent interactions are displayed at isosurfaces of 0.5 au. The color of the isosurface is varied according to the value of  $sign(\lambda_2)\rho$  with a color scale of -0.05 < ρ < 0.05 au, see ref. [51] for further details.

## Acknowledgements

The authors thank the Deutsche Forschungsgemeinschaft (DFG)-Projektnummer 182849149-SFB 953 „Synthetic Carbon Allotropes“ for financial support. The authors gratefully acknowledge the computational resources and support provided by the Erlangen Regional Computing Center (RRZE).

## Conflict of interest

The authors declare no conflict of interest.

**Keywords:** cycloparaphenylene · density functional calculations · fullerene (MA)LDI mass spectrometry · gas-phase chemistry · supramolecular chemistry

- [1] R. Jasti, J. Bhattacharjee, J. B. Neaton, C. R. Bertozzi, *J. Am. Chem. Soc.* **2008**, *130*, 17646–17647.
- [2] M. N. Jagadeesh, A. Makur, J. Chandrasekhar, *J. Mol. Model.* **2000**, *6*, 226–233.
- [3] S. Yamago, Y. Watanabe, T. Iwamoto, *Angew. Chem. Int. Ed.* **2010**, *49*, 757–759; *Angew. Chem.* **2010**, *122*, 769–771.
- [4] T. Iwamoto, Y. Watanabe, Y. Sakamoto, T. Suzuki, S. Yamago, *J. Am. Chem. Soc.* **2011**, *133*, 8354–8361.
- [5] T. J. Sisto, M. R. Golder, E. S. Hirst, R. Jasti, *J. Am. Chem. Soc.* **2011**, *133*, 15800–15802.
- [6] E. Kayahara, Y. Sakamoto, T. Suzuki, S. Yamago, *Org. Lett.* **2012**, *14*, 3284–3287.
- [7] J. L. Xia, R. Jasti, *Angew. Chem. Int. Ed.* **2012**, *51*, 2474–2476; *Angew. Chem.* **2012**, *124*, 2524–2526.
- [8] P. J. Evans, E. R. Darzi, R. Jasti, *Nat. Chem.* **2014**, *6*, 404–408.
- [9] E. Kayahara, V. K. Patel, S. Yamago, *J. Am. Chem. Soc.* **2014**, *136*, 2284–2287.
- [10] H. Omachi, S. Matsuura, Y. Segawa, K. Itami, *Angew. Chem. Int. Ed.* **2010**, *49*, 10202–10205; *Angew. Chem.* **2010**, *122*, 10400–10403.
- [11] M. R. Golder, B. M. Wong, R. Jasti, *Chem. Sci.* **2013**, *4*, 4285–4291.
- [12] H. Omachi, T. Nakayama, E. Takahashi, Y. Segawa, K. Itami, *Nat. Chem.* **2013**, *5*, 572–576.
- [13] S. Iijima, *Nature* **1991**, *354*, 56–58.
- [14] B. W. Smith, M. Monthieux, D. E. Luzzi, *Nature* **1998**, *396*, 323–324.
- [15] S. Fomine, M. G. Zolotukhin, P. Guadarrama, *J. Mol. Model.* **2012**, *18*, 4025–4032.
- [16] S. M. Bachrach, Z.-C. Zayat, *J. Org. Chem.* **2016**, *81*, 4559–4565.
- [17] S. Hashimoto, T. Iwamoto, D. Kurachi, E. Kayahara, S. Yamago, *ChemPlusChem* **2017**, *82*, 1015–1020.
- [18] Y. Xu, M. von Delius, *Angew. Chem. Int. Ed.* **2020**, *59*, 559–573; *Angew. Chem.* **2020**, *132*, 567–582.
- [19] K. Yuan, Y. J. Guo, X. Zhao, *J. Phys. Chem. C* **2015**, *119*, 5168–5179.
- [20] K. Yuan, C.-H. Zhou, Y.-C. Zhu, X. Zhao, *Phys. Chem. Chem. Phys.* **2015**, *17*, 18802–18812.
- [21] I. González-Veloso, J. Rodríguez-Otero, E. M. Cabaleiro-Lago, *Phys. Chem. Chem. Phys.* **2016**, *18*, 31670–31679.
- [22] J. Rio, D. Erbahar, M. Rayson, P. Briddon, C. P. Ewels, *Phys. Chem. Chem. Phys.* **2016**, *18*, 23257–23263.
- [23] T. Iwamoto, Y. Watanabe, T. Sadahiro, T. Haino, S. Yamago, *Angew. Chem. Int. Ed.* **2011**, *50*, 8342–8344.
- [24] J. Xia, J. W. Bacon, R. Jasti, *Chem. Sci.* **2012**, *3*, 3018–3021.
- [25] T. Iwamoto, Y. Watanabe, H. Takaya, T. Haino, N. Yasuda, S. Yamago, *Chem. Eur. J.* **2013**, *19*, 14061–14068.
- [26] T. Iwamoto, Z. Slanina, N. Mizorogi, J. D. Guo, T. Akasaka, S. Nagase, H. Takaya, N. Yasuda, T. Kato, S. Yamago, *Chem. Eur. J.* **2014**, *20*, 14403–14409.
- [27] H. Ueno, T. Nishihara, Y. Segawa, K. Itami, *Angew. Chem. Int. Ed.* **2015**, *54*, 3707–3711.
- [28] Y. Nakanishi, H. Omachi, S. Matsuura, Y. Miyata, R. Kitaura, Y. Segawa, K. Itami, H. Shinohara, *Angew. Chem. Int. Ed.* **2014**, *53*, 3102–3106.

- [29] D. Lu, G. Zhuang, H. Wu, S. Wang, S. Yang, P. Du, *Angew. Chem. Int. Ed.* **2017**, *56*, 158–162.
- [30] W. Zhang, A. Abdulkarim, F. E. Golling, H. J. Räder, K. Müllen, *Angew. Chem. Int. Ed.* **2017**, *56*, 2645–2648.
- [31] Y.-Y. Fan, D. Chen, Z.-A. Huang, J. Zhu, C.-H. Tung, L.-Z. Wu, H. Cong, *Nat. Commun.* **2018**, *9*, 3037.
- [32] Y. Segawa, M. Kuwayama, Y. Hijikata, M. Fushimi, T. Nishihara, J. Pirillo, J. Shirasaki, N. Kubota, K. Itami, *Science* **2019**, *365*, 272–276.
- [33] J. Rio, S. Beeck, G. Rotas, S. Ahles, D. Jacquemin, N. Tagmatarchis, C. Ewels, H. A. Wegner, *Angew. Chem. Int. Ed.* **2018**, *57*, 6930–6934.
- [34] A. Stergiou, J. Rio, J. H. Griwatz, D. Arçon, H. A. Wegner, C. P. Ewels, N. Tagmatarchis, *Angew. Chem. Int. Ed.* **2019**, *58*, 17745–17750.
- [35] P. W. Fowler, D. E. Manolopoulos, *An Atlas of Fullerenes*, Oxford: Clarendon Press, **1995**.
- [36] Y. Xu, B. Wang, R. Kaur, M. B. Minameyer, M. Bothe, T. Drewello, D. M. Guldi, M. von Delius, *Angew. Chem. Int. Ed.* **2018**, *57*, 11549–11553.
- [37] Y. Xu, R. Kaur, B. Wang, M. B. Minameyer, S. Gsänger, B. Meyer, T. Drewello, D. M. Guldi, M. von Delius, *J. Am. Chem. Soc.* **2018**, *140*, 13413–13420.
- [38] Y. Xu, S. Gsänger, M. B. Minameyer, I. Imaz, D. Maspoch, O. Shyshov, F. Schwer, X. Ribas, T. Drewello, B. Meyer, M. von Delius, *J. Am. Chem. Soc.* **2019**, *141*, 18500–18507.
- [39] D. Lungerich, J. F. Hitzemberger, M. Marcia, F. Hampel, T. Drewello, N. Jux, *Angew. Chem. Int. Ed.* **2014**, *53*, 12231–12235.
- [40] R. W. Kirschbaum, D. Prenzel, S. Frankenberger, R. R. Tykwinski, T. Drewello, *J. Phys. Chem. C* **2015**, *119*, 2861–2870.
- [41] I. D. Kellner, L. C. Nye, M. S. von Gernler, J. Li, M. D. Tzirakis, M. Orfanopoulos, T. Drewello, *Phys. Chem. Chem. Phys.* **2014**, *16*, 18982–18992.
- [42] D. Lungerich, J. F. Hitzemberger, W. Donaubaue, T. Drewello, N. Jux, *Chem. Eur. J.* **2016**, *22*, 16755–16759.
- [43] Turbomole V 7.0 **2015**, University of Karlsruhe and Forschungszentrum Karlsruhe GmbH 1989–2007, Turbomole GmbH since 2007.
- [44] J. P. Perdew, K. Burke, M. Ernzerhof, *Phys. Rev. Lett.* **1996**, *77*, 3865–3868.
- [45] A. D. Becke, *J. Chem. Phys.* **1993**, *98*, 5648–5652.
- [46] C. Lee, W. Yang, R. G. Parr, *Phys. Rev. B* **1988**, *37*, 785–789.
- [47] A. Schäfer, C. Huber, R. Ahlrichs, *J. Chem. Phys.* **1994**, *100*, 5829–5835.
- [48] M. Sierka, A. Hogekamp, R. Ahlrichs, *J. Chem. Phys.* **2003**, *118*, 9136–9148.
- [49] S. Grimme, J. Antony, S. Ehrlich, H. Krieg, *J. Chem. Phys.* **2010**, *132*, 154104.
- [50] S. Grimme, S. Ehrlich, L. Goerigk, *J. Comput. Chem.* **2011**, *32*, 1456–1465.
- [51] J. Contreras-García, E. R. Johnson, S. Keinan, R. Chaudret, J.-P. Piquemal, D. N. Beratan, W. Yang, *J. Chem. Theory Comput.* **2011**, *7*, 625–632.
- [52] B. M. Wong, *J. Phys. Chem. C* **2009**, *113*, 21921–21927.
- [53] U. Boesl, H. J. Neusser, E. W. Schlag, *Z. Naturforsch. Sect. A* **1978**, *33*, 1546–1548.
- [54] C. Yeretdzian, K. Hansen, F. Diederich, R. L. Whetten, *Nature* **1992**, *359*, 44–47.
- [55] D. Lungerich, J. F. Hitzemberger, F. Hampel, T. Drewello, N. Jux, *Chem. Eur. J.* **2018**, *24*, 15818–15824.
- [56] R. Arakawa, M. Kobayashi, T. Nishimura, *J. Mass Spectrom.* **2000**, *35*, 178–182.
- [57] C. Y. Airiau, R. G. Brenton, J. Crosby, *Rap. Commun. Mass Spectrom.* **2001**, *15*, 135–140.
- [58] N. Toriumi, A. Muranaka, E. Kayahara, S. Yamago, M. Uchiyama, *J. Am. Chem. Soc.* **2015**, *137*, 82–85.
- [59] M. Peña Alvarez, P. Mayorga Burrezo, T. Iwamoto, L. Qiu, M. Kertesz, M. Taravillo, V. G. Baonza, J. T. Lopez Navarrete, S. Yamago, J. Casado, *Faraday Discuss.* **2014**, *173*, 157–171.
- [60] R. K. Yoo, B. Ruscic, J. Berkowitz, *J. Chem. Phys.* **1992**, *96*, 911–918.

Manuscript received: March 28, 2020

Revised manuscript received: May 23, 2020

Accepted manuscript online: May 31, 2020

Version of record online: July 1, 2020